

Optimal Timing for In Vivo ^1H -MR Spectroscopic Imaging of the Human Prostate at 3T

Tom W.J. Scheenen,^{1*} Giulio Gambarota,¹ Elisabeth Weiland,^{2,3} Dennis W.J. Klomp,¹ Jurgen J. Fütterer,¹ Jelle O. Barentsz,¹ and Arend Heerschap¹

Proton MR spectroscopic imaging (^1H -MRSI) of the human prostate, which has an interesting clinical potential, may be improved by increasing the magnetic field strength from 1.5T to 3T. Both theoretical and practical considerations are necessary to optimize the pulse timing for spectroscopic imaging of the human prostate at 3T. For in vivo detection of the strongly coupled spin system of citrate, not only should the spectral shape of the signal be easy to identify, but the timing used should produce MR signals at reasonably short echo times (TEs). In this study the spectral shape of the methylene protons of citrate was simulated with density matrix calculations and checked with phantom measurements. Different calculated optimal spectral shapes were measured in patients with prostate cancer with a 2D spectroscopic imaging sequence. T_1 and T_2 relaxation times were calculated for citrate and choline, the two major metabolites of interest in the prostate. We conclude that the optimum timing for in vivo point-resolved spectroscopy (PRESS) imaging at 3T is an interpulse timing sequence of $90^\circ - 25 \text{ ms} - 180^\circ - 37.5 \text{ ms} - 180^\circ - 12.5 \text{ ms} - \text{echo}$. A short repetition time (TR) of 750 ms partially saturates choline signals, but increases the SNR per unit time for citrate, and accommodates a maximum number of weighted averages of an elliptically sampled k -space for accurate localization and minimal contamination of the individual spectra. This is illustrated by means of a 3D spectroscopic imaging experiment in a complete prostate in vivo. *Magn Reson Med* 53:1268–1274, 2005. © 2005 Wiley-Liss, Inc.

Key words: citrate; choline; relaxation times; AB spin system; density matrix; computer simulations

Whole-body scanners with a magnetic field strength of 3T are becoming more and more available to the scientific and clinical communities. With the construction of appropriate radiofrequency (RF) coils for different parts of the body, it becomes possible for researchers and clinicians to make full use of the increased sensitivity of a field strength of 3T compared to 1.5T. We have been using an endorectal coil for 3T to explore the possibilities of proton (^1H) MRI and MR spectroscopic imaging (MRSI) of the prostate at this field strength (1). In the continuing search for a non-invasive imaging technique that can reliably differentiate prostate cancer from benign prostatic hyperplasia and

healthy tissue, ^1H -MRSI has been shown to have great potential (2–4). In fact, prostate cancer tissue is characterized by reduced levels of citrate and increased levels of choline (5,6), which are both detectable in vivo with ^1H -MRSI.

The spin-spin coupling constant J and the chemical shift difference δ of the four methylene protons of citrate are of the same order of magnitude at 1.5 and at 3T, which means that the corresponding ^1H -spectral shape of these protons at these field strengths is an AB-type multiplet. The exact shape of this multiplet, centered at 2.60 ppm, depends not only on J and δ , but also on the type and timing of the RF pulses of the MR pulse sequence used. An optimal shape of the citrate AB spin system at echo time (TE) in a point-resolved spectroscopy (PRESS) (7) pulse sequence ($90_x - \tau_1 - 180_y - \tau_2 - 180_z - (\tau_2 - \tau_1)$ echo) was previously reported for 1.5T (8): with $\tau_1 = 11 \text{ ms}$ and $\tau_2 = 60 \text{ ms}$ ($\text{TE} = 2 \times \tau_2 = 120 \text{ ms}$), the outer lines of the multiplet almost completely disappear, whereas the inner lines of the multiplet have maximum absorptive intensity in the in-phase spectrum.

In addition to the spectral shape of citrate, the relaxation times of the relevant metabolites at 3T are also of interest. Optimal timing with regard to the spectral shape might not be optimal in terms of relaxation of the citrate or choline signal. The TE of the PRESS sequence should be smaller than or at least in the order of the T_2 relaxation time of citrate and choline to have sufficient signal left at TE. The T_1 relaxation time defines the optimum repetition time (TR) for a maximum signal-to-noise ratio (SNR) per unit time.

In this work we assessed the optimal timing for ^1H -MRSI of the prostate at 3T. For that purpose we simulated the spectral shape of the citrate methylene protons with density matrix calculations, and compared the theoretical spectra with in vitro measurements of a phantom containing a solution of citrate, creatine, and choline. Using different values for the pulse timing and TR, we measured the prostates of 10 patients with prostate cancer in vivo to estimate the T_1 and T_2 relaxation times of the relevant metabolites at 3T. We combined these findings to describe an optimal pulse sequence timing for 3D ^1H -MRSI of the prostate at 3T.

MATERIALS AND METHODS

Density Matrix Calculations

In this study, we developed a computer simulation program based on the density matrix formalism (9,10) to predict the spin dynamics of strongly coupled spin systems. As mentioned above, citrate is a strongly coupled AB spin system at 3T, and only a quantum mechanical treatment

¹Department of Radiology, University Medical Center Nijmegen, Nijmegen, The Netherlands.

²Siemens Medical Solutions, Erlangen, Germany.

³University of Bremen, Bremen, Germany.

Grant sponsor: Dutch Cancer Society.

*Correspondence to: Tom W.J. Scheenen, Department of Radiology (430), University Medical Center Nijmegen, Geert Grooteplein 10, 6525 GA Nijmegen, The Netherlands. E-mail: T.Scheenen@rad.umcn.nl

Received 16 February 2004; revised 20 December 2004; accepted 28 December 2004.

DOI 10.1002/mrm.20468

Published online in Wiley InterScience (www.interscience.wiley.com).

© 2005 Wiley-Liss, Inc.

can account for its complex dynamics. The Hamiltonian of citrate can be written as (11):

$$H = \omega_0(I_z + S_z) + \delta/2(I_z - S_z) + JI \cdot S \quad [1]$$

where I and S are the angular momentum operators for the A and B spins, respectively, ω_0 is the frequency at the main magnetic field strength, δ is the chemical shift between the two spins ($\delta = 18$ Hz at 3T), and J is the spin-spin coupling constant ($J = 15$ Hz) (12). In our code we assumed the pulses in the pulse timing scheme to be ideal, and we neglected T_2 relaxation effects. All of the angular momentum and rotation operators were represented by 4×4 matrices with complex elements in the product spin basis. We obtained the operators by taking the Kronecker products of the corresponding single spin operators. The simulated spectral-peak-absorption area of citrate, as well as the line shape as a function of τ_1 and TE over a range of 1–125 ms were then evaluated. More specifically, series of spectra with fixed τ_1 and varying TE were simulated.

Phantom Measurements

The spectral shape of citrate was measured in vitro with a PRESS measurement of a single voxel of $20 \times 20 \times 20$ mm in a glass sphere with an aqueous solution of citrate (90 mM) at a pH of 7.4. At two different values of τ_1 (10 and 25 ms) τ_2 was varied over a wide range of values, resulting in spectra at TEs of 50–205 ms. In these measurements, water signals were suppressed with a water suppression enhanced through T_1 effects (WET) scheme before excitation (13) (16 averages, TR = 1.5 s, acquisition time = 30 s).

Subjects and Hardware

Four weeks after transrectal ultrasound (US)-guided sextant biopsies were obtained, MRSI was performed in 10 untreated patients with histologically proven prostate cancer, after informed consent was obtained from the patients. The MR examinations were performed on a 3T MR scanner (Magnetom Trio; Siemens Medical Solutions, Erlangen, Germany). The body RF coil of the system was used for excitation, and a disposable endorectal coil (MRInnervu; Medrad Inc., Pittsburgh, PA, USA) was used for signal reception.

MR Acquisition Protocol

After a localizer and two fast turbo gradient spin-echo measurements were obtained for patient (or phantom) and coil positioning, a high-resolution T_2 -weighted turbo spin echo (TSE) pulse sequence was used in three directions for an anatomical overview of the prostate and surrounding tissues (effective TE = 109 ms, TR = ~4 s, field of view (FOV) = 180×90 mm, matrix size = 512×256 , 10–15 slices, thickness = 4 mm). Axial images in the patient were taken perpendicular to the rectal wall, to serve as proper background images for the measurement matrices of the MRSI experiments.

Several SI measurements with different TEs and TRs were obtained for each patient. We used 2D MRSI with relatively large voxel sizes to be able to perform six to eight

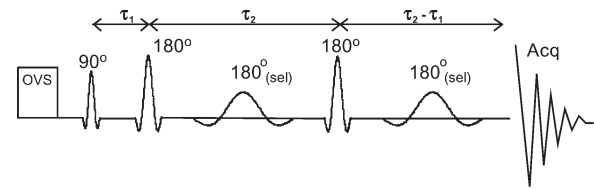


FIG. 1. Diagram of the RF pulses of the 2D ^1H -MRSI pulse sequence. Three slice-selective PRESS pulses with spacing $90_x - \tau_1 - 180_y - \tau_2 - 180_z - (\tau_2 - \tau_1) - \text{echo}$ produce an echo of the signal in the PRESS box at TE = $2\tau_2$ and two dual-band frequency-selective inversion pulses selectively invert and spoil water and lipid signals.

different SI experiments with different TEs and TRs in each patient within a tolerable amount of time (the MRSI part of the examination did not take more than 25 min). In the 2D ^1H -MRSI PRESS pulse sequence (Fig. 1) we used a nine-lobe sinc shape as a 90° pulse, and Mao-optimized 180° pulses with optimal slice profiles (14). Three selected combinations of the timing between the different pulses (τ_1 and τ_2 , and thus TE) were acquired to show the different spectral shapes of the citrate resonances in vivo and to calculate T_2 values. In addition to the TE, we also varied TR to estimate the T_1 relaxation times of the metabolites (other parameters: TR = 0.6, 1.2, and 2 s; FOV = 140×117 mm; matrix size = 12×10 , slice thickness = 10 mm, acquisition bandwidth = 1250 Hz, 512 spectral data points, and weighted k -space acquisition with three averages in the center of k -space). For in vivo SI measurements of the prostate, it is crucial to suppress both water and lipid resonances. Toward that end we used two dual-band frequency-selective Shinnar-LeRoux type 180° pulses with a duration of 12.8 ms (15), applied on both sides of either the first or second (depending on τ_1 and τ_2) slice-selective 180° Mao pulse, and surrounded by crushing gradients (i.e., the Mescher-Garwood water suppression (MEGA) (16), or double band-selective inversion with gradient dephasing (BASING) (17,18) technique). As a proof of principle we measured the prostate of one patient with acquisition-weighted 3D MRSI at a selected TE and TR to acquire spectra of the whole prostate in a single measurement.

Data Processing and Analysis

The acquisition-weighted 2D SI measurements were filtered in the two spatial dimensions with a Hanning filter, and zero-filled to a 16×16 matrix before they were Fourier transformed. The combination of a weighted acquisition and filtering of k -space reduced contamination from one voxel to the other, but increased the nominal voxel size by a factor of 1.71 in both directions (19).

To evaluate and quantify all of the individual spectra, we used the software package PRISMA (University of Bremen and Siemens Medical Solutions, Erlangen, Germany). Automated postprocessing of this software package consists of the following steps: 1) identification of the prominent metabolites by cross-correlation to a database (i.e., citrate, creatine, and choline in the prostate), 2) determination of the B_0 shift and starting values for the fit parameters, 3) residual water removal, and 4) complex fit to the

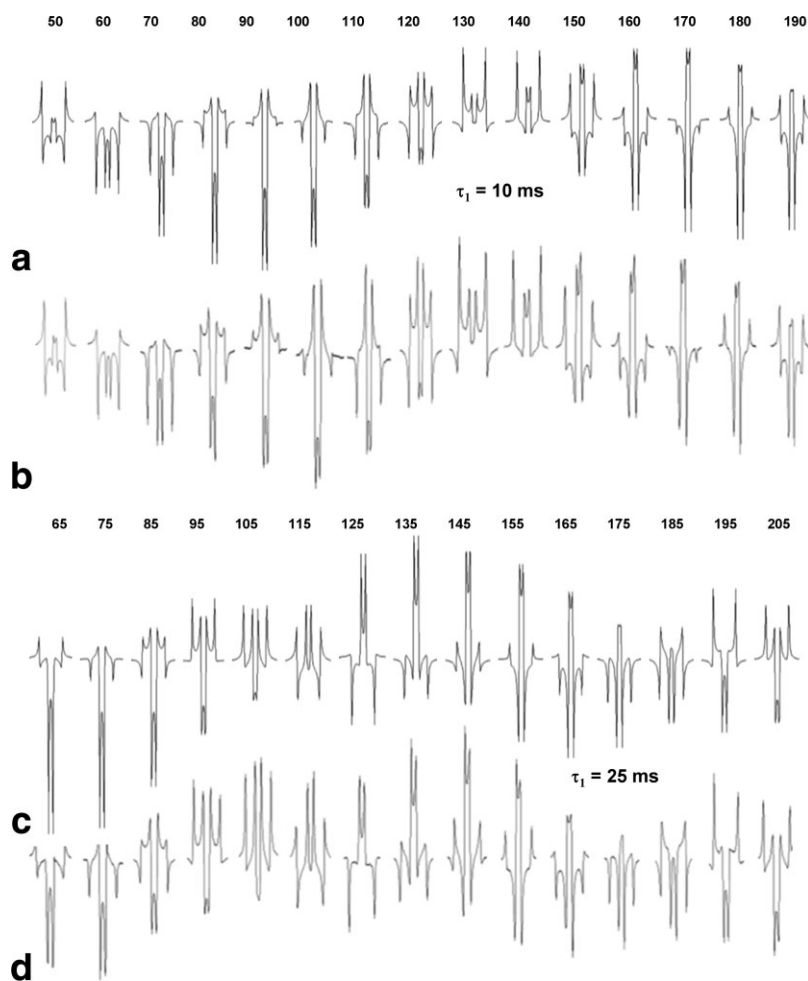


FIG. 2. Simulated and in vitro modulation of the spectral shape of the strongly coupled protons of citrate at 3T. In (a) simulation and (b) in vitro measurements τ_1 is set at 10 ms, and τ_2 is varied from 25 to 95 ms. In (c) simulation and (d) in vitro measurements τ_1 is set at 25 ms, and τ_2 is varied from 32.5 to 102.5 ms. The scale on the y-axis is fixed to show both the changes in spectral shape and relative signal intensities of the spectra as they evolve as a function of TE.

spectroscopic data in the time domain. The fit is based on a basis set of metabolic time signals, which are simulated quantum-mechanically with the use of literature values for chemical shifts and coupling constants. In addition, baseline artifacts are handled by truncating and remodeling the first data points.

We used one to three independent voxels of the MRS images of a patient to calculate integrals of the choline and citrate signals at different TEs and TRs to estimate the T_1 and T_2 relaxation times of these metabolites. To obtain an accurate fit of a T_2 value to the citrate integral as a function of TE, it is essential to take the modulation of this integral with TE into account. The software package takes this extra modulation into account when it calculates the relative amplitude of the citrate model spectrum. The resulting values for the citrate integral as a function of TE were then fitted to a single exponential decay curve (describing T_2 relaxation). T_1 values were estimated by fitting the choline and citrate integral (with incorporated TE modulation) as a function of TR to a simplified signal increase curve of the progressive saturation experiment.

RESULTS

Density Matrix Calculations and Phantom Measurements

To obtain a useful spectral shape of the citrate resonance, we calculated the integral of the spectrum and simulated

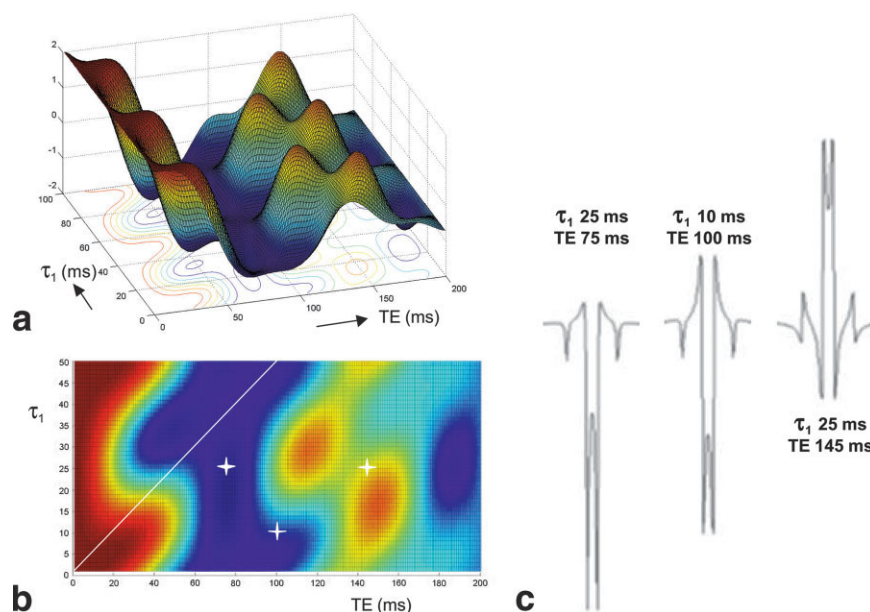
the shape as a function of pulse timing. In Fig. 2 the simulated evolution of the citrate spectrum as a function of TE is shown for two fixed values of τ_1 (10 ms in Fig. 2a, 25 ms in Fig. 2c), together with the corresponding in vitro measurements of the phantom with the citrate solution (Fig. 2b and d).

In addition to the spectral shape, the total integral of the spectrum changes dramatically with TE (without taking relaxation into account), as indicated in Fig. 3a and b. In Fig. 3c, three spectral shapes of citrate are presented with almost all intensity in the inner lines and a total integral of the spectrum close to a maximum or minimum value in Fig. 3a and b. At values for τ_1 , τ_2 , and TE of 25/37.5/75, 10/50/100 and 25/72.5/145 ms, respectively, two negative and one positive absorptive spectra are shown.

In Vivo Measurements of Citrate at 3T

At the selected values for pulse timing of the PRESS pulse sequence, we used 2D ^1H -MRSI to measure the metabolite signals in the prostate of patients with prostate cancer. In Fig. 4 the different spectral shapes of citrate are shown from the same location in one patient. The three spectral shapes (Fig. 4c–e) largely correspond to the theoretical shapes (Fig. 3c). From the longest TE (τ_1 25 ms, TE = 145 ms), the spectra of all voxels inside the prostate are shown in Fig. 4b. In addition to citrate, the spectral region

FIG. 3. Simulated modulation of the integral of the citrate signal at 3T. In **a** and **b** the total integral of the spectrum is indicated as a value of ± 2 , with 2 (arbitrary units) being the signal integral at excitation (relaxation is excluded in the simulations). Values of τ_1 exceeding half the TE are physically impossible, indicated with a solid white line in **b**. **c**: Three useful combinations of τ_1 and τ_2 are presented that result in effective TEs of 75, 100, and 145 ms.



from 3.00 to 3.25 ppm also showed large signal intensities, originating from creatine (3.04 ppm), choline (3.20 ppm), and possibly polyamines in between (Fig. 4c–e). The intensity of residual lipid signals below 2.5 ppm rapidly decreased with increasing TE. Regional differences in the metabolite signals were clear from the spectral map. The increased choline and decreased citrate signals in the left peripheral zone (Fig. 4b) suggest the presence of prostate cancer at this location.

Spectral Fitting and Relaxation Time Calculations

In four out of 10 patients the spectral data of the short-TE experiments (TE = 75 and 100 ms) were contaminated with residual lipid signals. In six patients we found voxels that could be fitted correctly for all different TEs and TRs for T_1 and T_2 evaluation. Figure 5 shows the results of fits to two spectra (TE = 145 ms) from different regions of the patient shown in Fig. 4. The green lines (Fig. 5a and b) represent the fitted metabolite signals, which are, together with the blue baselines, overlaid in red over the measured spectra (top black lines). The bottom black lines are the residuals, showing the difference between the fits and the measured spectra. There is a clear difference in the amount of choline relative to the amount of citrate between the two spectra.

As a measure for the integral of the citrate signal, we used the relative signal amplitude that was fitted to the citrate model function in the time domain. For choline, this corresponds to the signal intensity at $t = 0$ of the fitted signal in the time domain. Calculations of the relaxation times for citrate and choline could then be done straightforwardly with the values for the signal integrals. Depending on the number of available integral values for different TEs and TRs, the relaxation times were estimated either by a fit to (with three points) or a calculation of (when only two points were available) a monoexponential decay curve (T_2 relaxation) or a simplified signal increase curve of the progressive saturation experiment (T_1 relaxation). The

mean T_1 's of citrate and choline in the prostate at 3T were respectively 0.47 ± 0.14 s and 1.1 ± 0.4 s, whereas the mean T_2 values for choline and citrate were respectively 0.22 ± 0.09 s and 0.17 ± 0.05 s.

In a first attempt to show the possibilities of MRSI of the prostate, we measured the whole prostate of one patient with the use of 3D-MRSI at TE = 75 ms and TR = 750 ms. In Fig. 6 the spectral maps of two slices of this data set are shown. Despite the outer volume saturation (OVS) slabs and frequency-selective refocusing pulses that suppress water and lipid signals, there are still some residual lipid signals left close to the edges of the prostate. The linewidth at half height of the water signal over the complete PRESS-selected volume in this 3D measurement was ~ 36 Hz, which overrules the gain in spectral resolution of a field strength of 3T (compared to 1.5T). Nonetheless, the citrate signal can clearly be distinguished throughout most of the voxels. The linewidths for individual voxels are on the order of 10 Hz, which is too large to distinguish the splitting of the center lines of citrate (which are visible only when linewidths are below 8 Hz).

DISCUSSION

We simulated the spectral shape of the citrate AB spin system as a function of PRESS pulse timing at 3T, and found an excellent agreement between the simulated spectra and the spectra from in vitro measurements. The close similarity of the phantom measurements indicated that the simulations were correct (RF pulse durations may be neglected) and could be used to investigate an optimal spectral shape. Three options were presented in which the inner lines of the spectrum had a high absorptive intensity (negative for τ_1 25, TE = 75 ms, and τ_1 10, TE = 100 ms; and positive for τ_1 25, TE = 145 ms), whereas the outer lines had only a low intensity (absorptive for TE = 75, and dispersive for TE = 100 and 145 ms). The total integral of the citrate spectrum at these different TEs was close to a

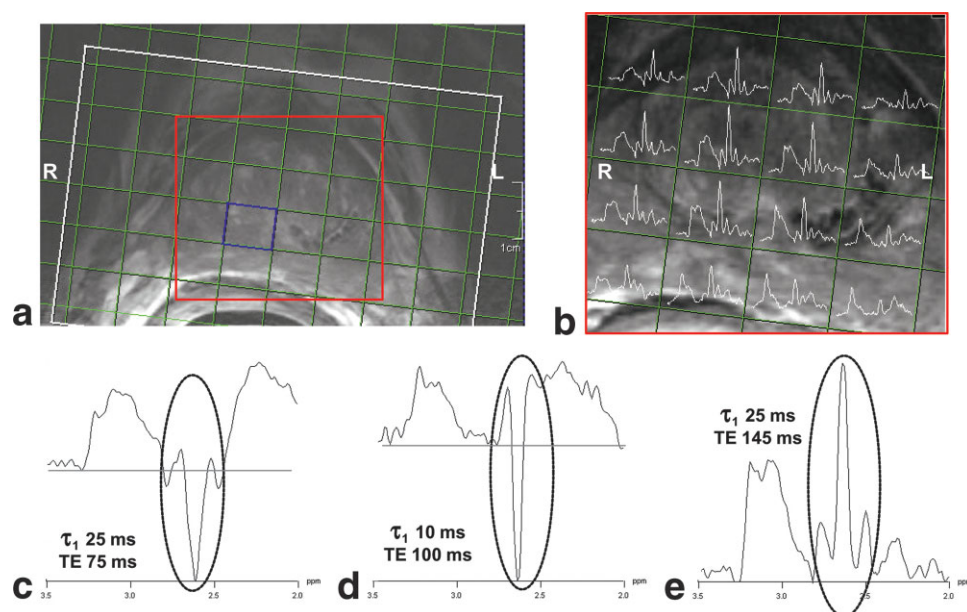


FIG. 4. Results of a 2D-MRSI examination of the prostate of a patient. **a**: T_2 -weighted TSE image of the prostate, on which the MRSI matrix is overlaid. Notice the angulation of the SI matrix for better coverage of the slightly tilted prostate. The white box indicates the PRESS-selection box. The red box is enlarged in **b**, in which for every voxel the spectrum is shown from 2.0 to 3.5 ppm at a TE of 145 ms. The blue voxel in **a** is the location of the spectra in **c–e**, acquired at TEs of 75, 100, and 145 ms, respectively. Measurement parameters: FOV = $140 \times 117 \times 10$ mm, matrix size = 12×10 , three weighted averages, TR = 600 ms (**c** and **d**) and 2000 ms (**e**), total measurement time = 1 min 6 s (**c** and **d**) and 3 min 26 s (**e**).

local minimum (TE = 75 and 100 ms) or maximum (TE = 145) in the evolution of the total citrate signal intensity as a function of τ_1 and TE (Fig. 3a and b). One advantage of these spectral shapes is that the intensity is concentrated in the inner lines, which makes it easier to detect in spectra with low SNR. The shape even allows an analysis with a simple Gaussian fit to the citrate signal, when more complicated model spectra are not at hand.

The spectral shape of citrate in the in vivo human prostate also corresponded largely to the theoretically simulated spectra. Possible differences between the in vivo and in vitro spectral shapes of citrate can be attributed to differences in linewidth and the presence of zinc ions in vivo, which influences the coupling constant of the citrate protons (12). Another source of differences may have been residual coil coupling of the endorectal coil in the in vivo measurement. The prototype interface between the endorectal coil and the scanner did not completely uncouple the endorectal coil while the PRESS pulse scheme was transmitted with the body coil, which may have caused deviating pulse angles close to the endorectal coil (on the order of 10–30%), which in turn may have changed the spectral shape of citrate locally. Locally increased RF amplitudes may also have influenced slice-selection profiles very close to the endorectal coil conductors (within 1 cm), possibly decreasing signal amplitudes inside the PRESS box, and increasing unwanted signals outside the PRESS box. To avoid exceeding the local specific absorption rate (SAR) because of this occasional residual coupling, we altered the SAR limits in the patient measurements to half the values set by the FDA.

Although we managed in all cases to position two dual-band frequency-selective refocusing pulses (to suppress

water and lipids in combination with crusher gradients) in the volume-selective PRESS pulse scheme, problems with lipid contamination in the spectra still occurred, especially at shorter TEs. One reason for this contamination is the inhomogeneity of the magnetic field in the prostate, which broadens the lipid resonances outside the ppm range that is refocused with the frequency-selective pulses. Another reason for residual lipid resonances is the size of the PRESS selection box, which had to be fairly large around the prostate because of the use of 180° RF pulses with a long duration (10 ms) to circumvent a chemical shift artifact during excitation. The RF amplifier used

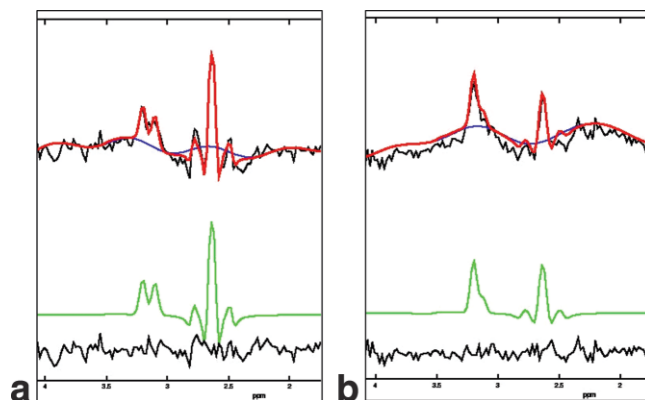
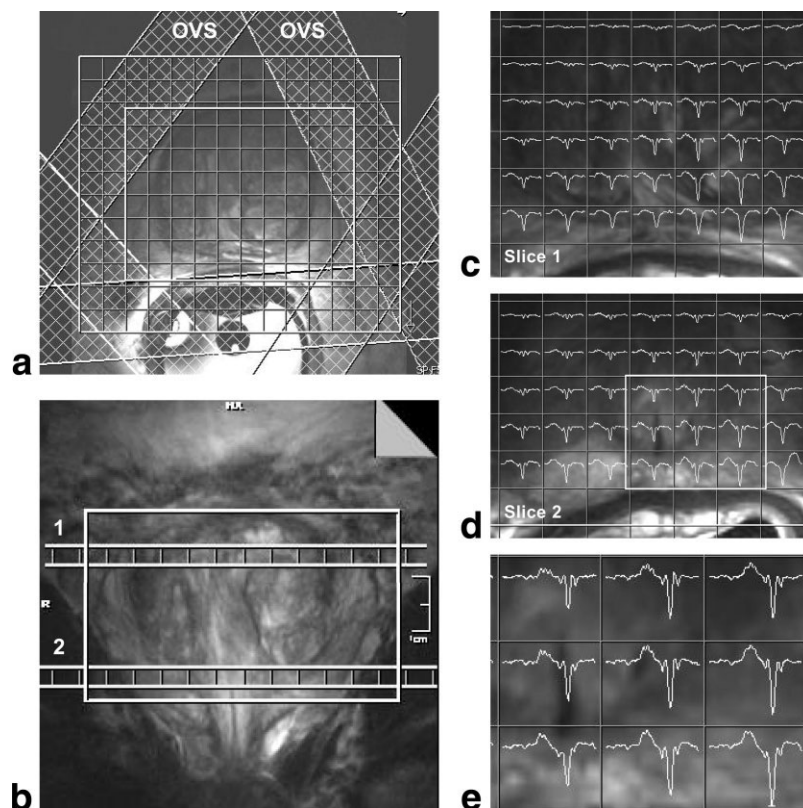


FIG. 5. Spectral fits of data for two voxels at TE = 145 ms of a patient with prostate cancer, with the PRISMA data processing program. **a** and **b**: (Top to bottom) measured spectrum (black) overlaid with the fit (red) and baseline (blue), metabolite fit (green), residual between data and fit (black).

FIG. 6. 3D-MRSI of a whole human prostate in vivo at 3T. (a) Axial and (b) coronal T_2 -weighted TSE images of the prostate are shown with the location of the OVS slabs, the volume selection with the PRESS pulses in white, and the actual acquisition matrix and the location of the two slices enlarged in c and d. From the total spectral width (1250 Hz), only the range from 2.0 to 3.5 ppm is shown in the individual spectra in the spectral maps (c and d). A block of nine voxels of the spectral map in d is enlarged in e to assess individual spectra (range = 2.0–4.0 ppm). The resolution of the spectral maps (the voxel size) is higher than the true resolution, because the original $14 \times 12 \times 10$ matrix was zero-filled to $16 \times 16 \times 16$ after filtering was performed with a 100% Hanning filter in three directions. Measurement parameters: TE = 75 ms, FOV = $84 \times 72 \times 60$ mm, matrix size = $14 \times 12 \times 10$, 3 weighted averages, TR = 750 ms, total measurement time = 8 min 17 s.



in this study did not have enough power to produce shorter RF pulses, by which the chemical shift artifact would decrease. Because of the large PRESS selection box used, some lipid tissue was present inside the PRESS box. Despite of the use of OVS slabs and frequency-selective water and lipid suppression, this tissue often contaminated the spectral region of citrate (about 2.6 ppm) and even choline (at 3.2 ppm). In future work these problems can be solved by improved interface decoupling circuitry and increased RF transmit power.

The PRISMA software package provided a semiautomatic fit to the individual spectra. Although the amount of voxels that had a good spectral quality throughout all different TEs and TRs, and originated from one location inside the prostate was limited, we were still able to extract relaxation times for both choline and citrate at 3T. Since the voxels were fairly large, and partial volume effects can be caused by imaging just one slice through the prostate, we were not able to discriminate between tumor and nontumor voxels in the presentation of the calculated relaxation times.

As expected, the calculated T_1 of citrate of 0.47 ± 0.14 s was larger than the reported apparent T_1 value of citrate in the human prostate at 1.5T of 0.34 ± 0.04 (measurements acquired in young volunteers) (3). In addition, an increase in T_1 from 0.84 ± 0.09 at 1.5T (3) to 1.1 ± 0.4 s at 3T was calculated for choline. The standard deviations (SDs) of the T_1 and T_2 values were large, similar to reported values for SDs of relaxation times of metabolites in the brain (20) and breast (21). This may reflect the technical challenge of acquiring these measurements, or the large interindividual differences that may exist. To avoid any influence from the

occasional residual coil coupling, we did not choose voxels whose spectra were used to calculate the T_1 and T_2 values of the metabolites that were on or adjacent to the endorectal coil conductors. To accommodate all OVS slabs and a data acquisition period of 410 ms (512 points at 1250 Hz) after the proposed TEs, we suggest the use of a TR of about 750 ms for MRSI of the prostate at 3T. With this TR one can take full advantage of the short T_1 value of citrate and partially saturate the choline resonance. The use of TR = 750 ms instead of, e.g., 1500 ms would increase the SNR per unit time with 17% for citrate, and decrease the SNR per unit time with 6% for choline, based on the estimated T_1 relaxation times. For a weighted averaged acquisition scheme in MRSI, it is advantageous to choose as short a TR as possible. With a short TR one can acquire more averages in the center of k -space within an acceptable measurement time, so the acquisition of the different phase-encode steps in k -space can be matched with the Hanning filter that is used to optimize the point spread function of all individual pixels. This prevents significant contamination from one voxel to the other, and accurately localizes spectra to their corresponding voxels (19,22). The partial saturation of the choline signal will decrease values for the choline/citrate ratio, which is used as a marker to differentiate cancer from healthy prostate tissue (5,6). Typical values for this ratio for healthy and tumor tissues should be reexamined at 3T. The calculated T_2 values of 0.22 ± 0.09 s for choline, and 0.17 ± 0.05 s for citrate do not significantly differ from the values at 1.5T (0.23 ± 0.06 s for choline (3), and an averaged apparent T_2 value of 0.13 ± 0.03 s for citrate in the whole prostate (23)), but they emphasize the need to choose a short TE in MRSI

of the prostate at 3T. Of the three selected TEs, the shortest one (τ_1 , τ_2 , and TE = 25/37.5/75 ms, respectively) is preferable, if localization and lipid suppression are adequate enough to produce uncontaminated spectra for all voxels in the prostate. This is illustrated with the 3D-MRS image of a patient in which the spectra throughout the prostate show citrate signals in voxels with a nominal size of $6 \times 6 \times 6$ mm (filtering is not accounted for) in a total measurement time of 8 min 17 s. The linewidth at half height of the water signal over the complete PRESS-selected volume in this measurement was ~ 36 Hz, which in future work should be decreased to fully exploit the advantages of 3D-MRSI at 3T.

CONCLUSIONS

This exploration of ^1H -MRSI of the prostate at a magnetic field strength of 3T involved both theoretical and practical considerations. Theoretically simulated shapes of the citrate spectrum corresponded with actual *in vitro* and *in vivo* measurements of the citrate signal. With this validation, the theory was used to calculate three optimal shapes of the citrate resonance, in which the total integral of the spectrum was close to a maximum or minimum, and the intensity of the outer lines of the spectral shape was minimal.

For practical purposes, the optimum spectral shape is not the only factor of interest—the TE at which this spectral shape occurs, and the TR that can be used are also important. From the calculated T_2 values of citrate and choline in the prostate *in vivo* at 3T, we can conclude that the TE in MRSI of the prostate at 3T must be short (75 ms). The choice of a short TR (750 ms) increases the SNR per unit time for citrate and partially saturates choline signals, but accommodates a maximum number of weighted averages of an elliptically sampled k -space for accurate localization and minimal contamination of the individual spectra. In MRSI of the human prostate, an adequate suppression of lipid signals and a locally homogeneous magnetic field are crucial, especially with the selected timing at this magnetic field strength.

ACKNOWLEDGMENTS

The authors thank George Misic (Medrad, Pittsburgh, PA, USA) for providing technical support and supplying the 3T endorectal coil and interface. The authors also acknowledge Stefan Röhl and Uwe Boettcher (Siemens Medical Solutions, Erlangen, Germany) for their help in programming the pulse sequences.

REFERENCES

- Fütterer JJ, Scheenen TWJ, Huisman HJ, Klomp DWJ, van Dorsten FA, Hulsbergen-van de Kaa CA, Witjes JA, Heerschap A, Barentsz JO. Initial experience of 3 Tesla endorectal coil magnetic resonance imaging and ^1H -spectroscopic imaging of the prostate. *Invest Radiol* 2004;39:671–680.
- Kurhanewicz J, Vigneron DB, Hricak H, Narayan P, Carroll P, Nelson SJ. Three-dimensional H-1 MR spectroscopic imaging of the *in situ* human prostate with high (0.24–0.7-cm³) spatial resolution. *Radiology* 1996;198:795–805.
- Heerschap A, Jager GJ, van der Graaf M, Barentsz JO, Ruijs SH. Proton MR spectroscopy of the normal human prostate with an endorectal coil and a double spin-echo pulse sequence. *Magn Reson Med* 1997;37:204–213.
- Kurhanewicz J, Swanson MG, Wood PJ, Vigneron DB. Magnetic resonance imaging and spectroscopic imaging: improved patient selection and potential for metabolic intermediate endpoints in prostate cancer chemoprevention trials. *Urology* 2001;57:124–128.
- Kurhanewicz J, Vigneron DB, Nelson SJ, Hricak H, MacDonald JM, Konety B, Narayan P. Citrate as an *in vivo* marker to discriminate prostate cancer from benign prostatic hyperplasia and normal prostate peripheral zone: detection via localized proton spectroscopy. *Urology* 1995;45:459–466.
- Heerschap A, Jager GJ, van der Graaf M, Barentsz JO, de la Rosette JJ, Oosterhof GO, Ruijter ET, Ruijs SH. *In vivo* proton MR spectroscopy reveals altered metabolite content in malignant prostate tissue. *Anticancer Res* 1997;17:1455–1460.
- Bottomley PA. Spatial localization in NMR spectroscopy *in vivo*. *Ann NY Acad Sci* 1987;508:333–348.
- van der Graaf M, Jager GJ, Heerschap A. Removal of the outer lines of the citrate multiplet in proton magnetic resonance spectra of the prostatic gland by accurate timing of a point-resolved spectroscopy pulse sequence. *MAGMA* 1997;5:65–69.
- Mulkern RV, Bowers JL. Density matrix calculations of AB spectra from multipulse sequences: quantum mechanics meets *in vivo* spectroscopy. *Concepts Magn Reson* 1994;6:1–23.
- Stables LA, Kennan RP, Anderson AW, Gore JC. Density matrix simulations of the effects of J coupling in spin echo and fast spin echo imaging. *J Magn Reson* 1999;140:305–314.
- Mulkern RV, Bowers JL, Peled S, Kraft RA, Williamson DS. Citrate signal enhancement with a homonuclear J-refocusing modification to double-echo PRESS sequences. *Magn Reson Med* 1996;36:775–780.
- van der Graaf M, Heerschap A. Effect of cation binding on the proton chemical shifts and the spin-spin coupling constant of citrate. *J Magn Reson B* 1996;112:58–62.
- Ogg RJ, Kingsley PB, Taylor JS. WET, a T1- and B1-insensitive water-suppression method for *in vivo* localized ^1H NMR spectroscopy. *J Magn Reson B* 1994;104:1–10.
- Mao J, Mareci TH, Andrew ER. Experimental study of optimal selective 180 radiofrequency pulses. *J Magn Reson* 1988;79:1–10.
- Pauly J, Le Roux P, Nishimura D, Macovski A. Parameter relations for the Shinnar-Le Roux selective excitation pulse design algorithm. *IEEE Trans Med Imaging* 1991;10:53–65.
- Mescher M, Tannus A, Johnson MO, Garwood M. Solvent suppression using selective echo dephasing. *J Magn Reson A* 1996;123:226–229.
- Males RG, Vigneron DB, Star Lack O, Falbo SC, Nelson SJ, Hricak H, Kurhanewicz J. Clinical application of BASING and spectral/spatial water and lipid suppression pulses for prostate cancer staging and localization by *in vivo* 3D H-1 magnetic resonance spectroscopic imaging. *Magn Reson Med* 2000;43:17–22.
- Star-Lack J, Nelson SJ, Kurhanewicz J, Huang LR, Vigneron DB. Improved water and lipid suppression for 3D PRESS CSI using RF band selective inversion with gradient dephasing (BASING). *Magn Reson Med* 1997;38:311–321.
- Pohmann R, von Kienlin M. Accurate phosphorus metabolite images of the human heart by 3D acquisition-weighted CSI. *Magn Reson Med* 2001;45:817–826.
- Ethofer T, Mader I, Seeger U, Helms G, Erb M, Grodd W, Ludolph A, Klose U. Comparison of longitudinal metabolite relaxation times in different regions of the human brain at 1.5 and 3 Tesla. *Magn Reson Med* 2003;50:1296–1301.
- Bolan PJ, Meisamy S, Baker EH, Lin J, Emory T, Nelson M, Everson LI, Yee D, Garwood M. *In vivo* quantification of choline compounds in the breast with ^1H MR spectroscopy. *Magn Reson Med* 2003;50:1134–1143.
- Scheenen TWJ, Klomp DWJ, Röhl SA, Fütterer JJ, Barentsz JO, Heerschap A. Fast acquisition-weighted three-dimensional proton MR spectroscopic imaging of the human prostate. *Magn Reson Med* 2004;52:80–88.
- Lowry M, Liney GP, Turnbull LW, Manton DJ, Blackband SJ, Horsman A. Quantification of citrate concentration in the prostate by proton magnetic resonance spectroscopy: zonal and age-related differences. *Magn Reson Med* 1996;36:352–358.